ACS OMEGA

http://pubs.acs.org/journal/acsodf

Article

Study on Synthesis and Adsorption Properties of ReO_4^- Ion-Imprinted Polymer

Pu Liu,[⊥] Weiwei Jia,[⊥] Xiaojian Ou, Chunli Liu, Jun Zhang, Zhenbin Chen,* and Xiaoming Li

Cite This: *ACS Omega* 2020, 5, 24356−24366

Read Online

ACCESS | Metrics & More | Article Recommendations | Supporting Information

ABSTRACT: In this work, an ion imprinted polymer (ReO_4^--IIP) of the perrhenate ion based on acrylamide (AM) and acrylic acid (AA) was prepared by solution polymerization using ReO_4^- as a template ion, *N*,*N*-methylenebisacrylamide (NMBA) as cross-linkers, hydrogen peroxide-vitamin C (H_2O_2-Vc) as an initiator, and a mixed solution of water (H_2O) and methanol (CH_3OH) with volume ratio v(H_2O)/v(CH_3OH) = 3:7 as a solvent. During the process of synthesis condition investigation and optimization, the adsorption capacity (Q) and the separation degree (R) in the equimolar concentration mixture solutions of NH_4ReO_4 and $KMnO_4$ were adopted as indexes, and the obtained optimal conditions were as follows: the molar ratios of NMBA, NH_4ReO_4, AA, H_2O_2, and Vc to AM were 5.73, 0.052, 1.29, 0.02, and 0.003, and the temperature and time of polymerization were 40 °C and 28 h, respectively. Under optimal conditions, the sample with indexes, Q and R of 0.064 mmol/g and 3.20, were harvested. What is more, a further reusability study found that good adsorption selectivity was maintained after repeating the experiment 9 times. Taking the non-IP prepared under the same conditions as a control, Fourier transform infrared spectroscopy, transmission electron microscopy, and Brunauer Emmett Teller were used to characterize the structure of the ReO_4^--IIP prepared under the optimal conditions. Finally, the kinetic study results showed that the zero-order kinetic model could better describe the adsorption process. The thermodynamic study results showed that the Langmuir model was more suitable for describing the isotherm adsorption process of the IIP.

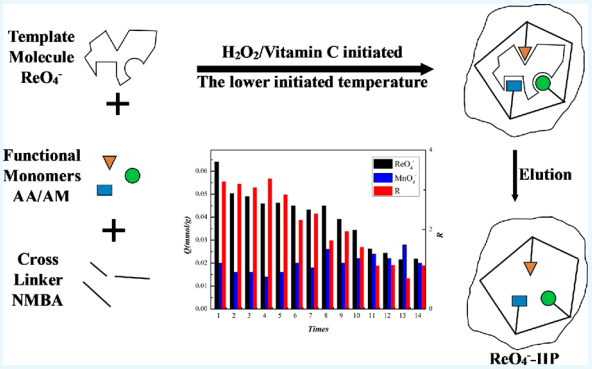

1. INTRODUCTION

With the rapid development of the defense, aerospace, and other industries, higher temperature-resistance requirements were imposed on the superalloys. In order to meet requirements of high temperature resistance, various superalloy elements were added.[1] Among which, rhenium (Re), a rare metal material, was widely favored because it could significantly improve the high temperature resistance.[2] Thus, Re had been introduced into a superalloy since the second generation of superalloys had been developed.[3,4] What is more, the quantities kept increasing continuously with the development of superalloy generation.[5] At present, Re introduced into a superalloy had arrived at about 6%, which meant huge amount of Re would be needed.[6] However, reserves of Re in the nature were seriously insufficient, and the quality of minerals was low, added to the extreme imbalance of minerals in distribution, the shortage of Re existed extensively naturally, which had impeded the development of superalloy industries and downstream industries seriously.[7] On the other hand, the metallurgical process of Re was not reasonable enough because the separation and purification was much inefficient. The separation and purification process was undertaken by the ion exchange method mainly for the moment, but the selectivity of this method was very poor.[8,9] Thus, many other assistant conduction ways, such as precipitation, extraction, recrystallization, etc., need to be included to ensure the demands of necessary purity, which would result in the long process route and low efficiency naturally. Therefore, developing a novel separation material and the related technology to achieve accurate separation to improve the separation and purification efficiency of Re from complex environments was urgently needed.

Imprinting technology, due to the special preparation process of an imprinted polymer (IP), possessed the specific template recognition property, and it was expected to accurately separate the template from complex environments. Besides, based on the special preparation process also, the IP had advantages of the long-term stability, structural presupposition, and wide applicability[10−12] and had become a research hotspot in the field of separation and purification.[13] As a

Received: June 3, 2020
Accepted: September 3, 2020
Published: September 16, 2020

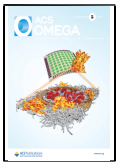

representative high-level adsorption material with good selectivity, the ion imprinted polymer (IIP) is a developed separation material on the basis of the molecular imprinting technology recently.[14−19] For the preparation process is simple and the selectivity for specific ions is excellent and adsorption capacity is large, the material has developed rapidly in the field of adsorption and has been widely used.[20,21] At present, in the process of synthesizing IIP, due to the few types of traditional functional monomers, the synthesized IIP has a low binding capacity, performance does not meet the ideal requirements, and postprocessing is relatively complicated.[22,23] In the process of using an IIP, there are some problems such as low adsorption capacity, weak recognition ability, difficult desorption, and poor reusability which are caused by problems in the selection and dosage of a cross-linking agent, functional monomer, solvent, and so forth.[24,25] Therefore, the challenge in the future is how to choose a suitable imprinting system and synthesize an IIP with excellent adsorption and desorption performance, strong recognition ability, and good reusability through simple operations.[26,27] An IIP was generally required to have a high degree of cross-linking (>80%) to ensure the strong rigidity to maintain the shape and integrity of the imprinted cavities.[28−30] Because ReO_4^- was a water-soluble target, an IIP focused on it should be prepared in an aqueous solution.[31,32] However, there was no suitable cross-linker to meet the demand because all of the frequently-used cross-linker could not resolve in water with so high solubility.[33,34] Besides, the accurate separation could not be ensured because the assembly among target ion and functional groups of monomers was mainly realized by the hydrogen bond, but the existence of water would weaken the assembly by competing functional groups with the target ion.[35,36] Thus, how to introduce a cross-linker with a high feed ratio and how to improve the selectivity would be key problems of this work.[37]

Through the previous study,[38,39] we found that when the mixed solution of water and methanol was used, the solubility of *N*,*N*-methylenebisacrylamide (NMBA) would increase to a great degree, which could ensure the cross-linking demand enough and make the shape retention and the cavity integrity of IP improved, and the selectivity of IP was elevated correspondingly. According to this experience, the mixture solution was chosen as a solvent in the ReO_4^--IIP preparation process. Both acrylamide (AM) and acrylic acid (AA) can self-assemble with template ions, ReO_4^-, which can increase the rigidity of the IIP, maintain the shape of the imprinted hole, and improve the performance of the IIP. In other words, they are functional monomers. The ReO_4^- is the template ion, which can exhibit a synergistic effect and make a better self-assemble structure and further lead to the higher specific adsorption.[40] After that, traditional preparation methods of the IIP usually require a higher temperature for initiation,[41] and this experiment can be carried out at a lower temperature using Vc-H_2O_2 as the initiator system. Besides, to further study the selectivity, this work conscripted the permanganate ion (MnO_4^-), which was similar in spatial structure and interatomic interaction with ReO_4^-, but possessed smaller size, and was selected as interference in condition investigation and optimization process using indexes of *Q* and *R* of ReO_4^--IIP to ReO_4^-,[42−44] and results documented that the molar ratios of NMBA, NH_4ReO_4, AA, H_2O_2, and Vc to AM were 5.73, 0.052, 1.29, 0.02 and 0.003, the temperature and time of polymerization were 40 °C and 28 h, and *Q* and *R* were 0.064 mmol/g and 3.20, respectively. What is more, good adsorption selectivity was maintained after repeating the experiment 9 times. Finally, based on the sample obtained under optimal conditions, the structure and morphology of the IIP were characterized with the NIIP as a reference, and the adsorption thermodynamics and kinetics were explored.

2. RESULTS AND DISCUSSION

2.1. Structural Characterization. The dried ReO_4^--IIP, NIIP, adsorbed ReO_4^--IIP (used IIP), and ReO_4^--IIP that were repeatedly used 9 times (reused IIP) were characterized by infrared spectroscopy. The infrared spectra of ReO_4^--IIP (includes unused, used, and reused IIP) and NIIP are shown in Figure 1. The peak at 3437.77 cm^{-1} was the stretching

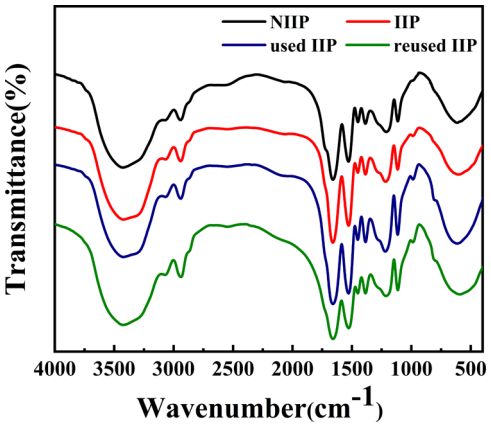

Figure 1. FTIR spectra of NIIP, ReO_4^--IIP, ReO_4^--IIP after adsorption (used IIP), and ReO_4^--IIP that has been reused nine times (reused IIP).

vibration peak of O−H in AA and N−H in AM, the peak at 2925.77 cm^{-1} was the stretching vibration peak of methyl or methylene in AM, NMBA, and AA, the peak at 1718.39 cm^{-1} could be ascribed to the stretching vibration peak of carbonyl in AM, NMBA, and AA, the peak at 1536.50 cm^{-1} was the deformation vibration peak of N−H in AM, the peak at 1453.19 cm^{-1} could be attributed to the deformation vibration of methyl or methylene groups in AA, NMBA, and AM, and the peak at 1394.96 cm^{-1} could be ascribed to O−H in AA and O═C−NH_2 in AM. Because of the asymmetric stretching vibration of C−O in O═C−O, an absorption peak appears at 1167.36 and 793.86 cm^{-1} that could be attributed to the rocking vibration of C−H and N−H in AA, NMBA, and AM. In summary, both ReO_4^--IIP and NIIP were the copolymers of AA, NMBA, and AM. As can be seen from the figure, the characteristic absorption peaks of the NIIP and IIP are basically the same, proving that they belong to the same type of copolymer.[45,46] The difference between the IIP and NIIP in structure could be deduced by absorption peaks at 1453.19, 1111.21, 934.94, and 507.17 cm^{-1} in the IIP shifted to 1450.32, 1106.93, 930.54, and 494.32 cm^{-1} in the NIIP. The synergistic effect of AA and AM on the surface of the imprinted hole resulted in the shift of the absorption peak. More importantly, the peak value at 814 cm^{-1} of Re−O tensile vibration can be assigned to the used and reused IIP, however, it was not observed in the IIP and NIIP. The reused IIP contrasted with the used IIP, and there were no changes in spectra, which could show that the IIP had good stability. The adsorption mechanism is shown in Scheme 1.

https://dx.doi.org/10.1021/acsomega.0c02634
ACS Omega 2020, 5, 24356−24366

Scheme 1. Adsorption Mechanism of ReO_4^--IIP

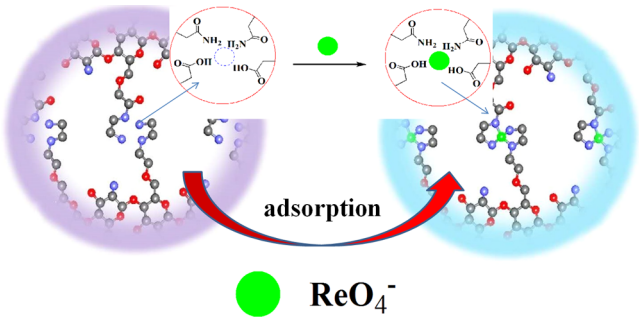

In order to further characterize the difference in morphology between the IIP and NIIP, the surface morphology of the IIP and NIIP was characterized by scanning electron microscopy (SEM) and transmission electron microscopy (TEM). SEM and TEM results of the IIP and NIIP are shown in Figure 2.

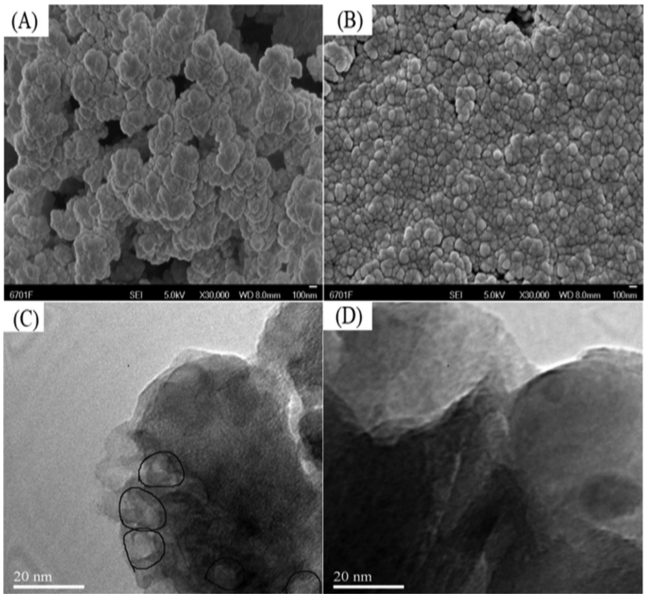

Figure 2. SEM images of (A) ReO_4^--IIP and (B) NIIP; TEM images of (C) ReO_4^--IIP and (D) NIIP.

From Figure 2A, it could be found that the surface of the IIP was relatively loose and many pores could be seen, while Figure 2B shows that the structure of the NIIP was piled with a compact way and almost no pores could be found. The obvious difference between the IIP and NIIP in morphology indicated the difference between the IIP and NIIP in the matrix structure and implied that ReO_4^--imprinted pores existed and a specific binding site of ReO_4^- was formed in the IIP.[47] TEM results in Figure 2C,D documented obvious imprinted cavities in the IIP (see marks in the figure), while almost no holes were found in the NIIP. Because the mixture solvent of methanol and water was conscripted in the ReO_4^--IIP synthesis process, and both of them could also combine with template ions and participate in self-assembly in the form of the hydrogen bond; thus, it can be calculated according to the theoretical model and the size of the imprinting cavity is larger than that of ReO_4^-. What is more, calculation found that if the size of H_2O (or CH_3OH) along the vertices of four-sided pyramids was added, the size of ReO_4^- was almost the same as that of imprinted cavities, which, at a certain degree, verified that water had combined with template ions and participated in self-assembly.[48] Besides, some cavities showed morphology different from the others, which could be ascribed to the subsequent reflow extraction of template ions, and drying of the IIP changed the shape of the imprinted cavities.

The Brunauer Emmett Teller (BET) method could be used to evaluate the differences of structures between the IIP and NIIP. Table 1 shows the pore size distribution (V_p), average pore width (d_p), and specific surface area (S_{BET}), which were calculated by the BET method. The results showed that V_p and d_p of the IIP were 181.5081 m^2/g and 16.4197 nm, respectively. The V_p and d_p of the NIIP were 40.5574 m^2/g and 13.4909 nm, respectively. The low V_p and d_p of NIIP were due to the highly hydrophilic effect of the functional groups, which lead to the pore shrinkage and collapse.

Table 1. Physical Characteristic Items of ReO_4^--IIP and NIIP from BET

items	unit	IIP	NIIP
S_{BET}	m^2/g	181.5081	40.5574
V_p	cm^3/g	0.7511	0.2039
d_p	nm	16.4197	13.4909

2.2. Adsorption Kinetics of ReO_4^--IIP. The relationship between the adsorption amount (Q_t) and the adsorption time (t) is shown in Figure 3. Q_t increases with the monotonic extension of t until it reaches adsorption equilibrium after 330 min. Because of the feature of the solution, imprinted cavities were distributed uniformly in the network of the IIP; thus, the adsorption would take place in a step-by-step manner until all ranges of particles were permeated, and Q_t increased monotonously with t and then kept constant naturally. Besides, because the interaction between imprinted cavities and ReO_4^- was a special physical interaction, the adsorption was a revisable process naturally, which meant that there was equilibrium between adsorption and desorption. As all ranges of IIP networks were permeated, the quantity of imprinted cavities would not increase again and the equilibrium would rise to the main factor of adsorption. According to the

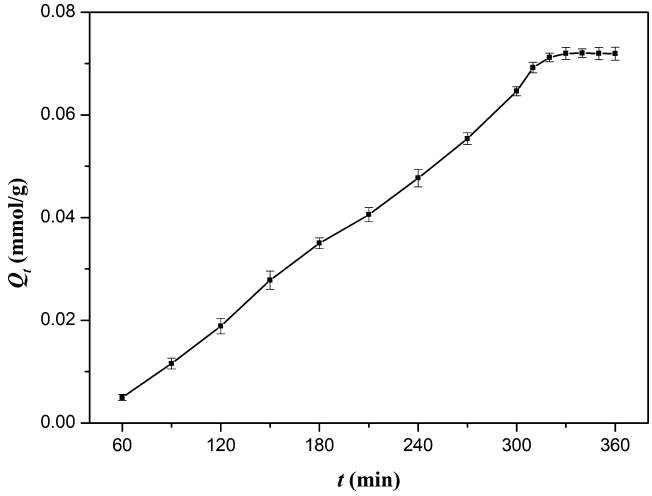

Figure 3. Relationship between adsorption capacity and adsorption time.

https://dx.doi.org/10.1021/acsomega.0c02634
ACS Omega 2020, 5, 24356−24366

principal of equilibrium, a constant of Q_t could be obtained naturally.

In order to further study the kinetics of the adsorption process, the zero-order model, pseudo-first-order model, and pseudo-second-order model[49] were used to analyze the adsorption kinetics data.

The zero-order model

$$\frac{dQ_t}{dt} = K_0 \tag{1}$$

in the formula, Q_t (mmol/g) is the amount of ReO_4^- adsorbed at time t and K_0 is the zero-order rate constant.

By integrating eq 2, eq 3 was obtained.

$$Q_t = K_0 t \tag{2}$$

The pseudo-first-order model

$$\frac{dQ_t}{dt} = K_1(Q_e - Q_t) \tag{3}$$

where Q_e is the amount of ReO_4^- adsorbed at equilibrium time (t_e) and K_1 is the pseudo-first-order rate constant. By integrating eq 3 under the boundary conditions $Q_t = 0$ at $t = 0$ and $Q_t = Q_t$ at time t, eq 4 was obtained.

$$\ln(Q_e - Q_t) = \ln Q_e - K_1 t \tag{4}$$

The pseudo-second-order model

$$\frac{dQ_t}{dt} = K_2(Q_e - Q_t)^2 \tag{5}$$

where K_2 is the rate constant of the pseudo-second-order model. By integrating eq 5 under the boundary conditions $Q_t = 0$ at $t = 0$ and $Q_t = Q_t$ at time t, eq 6 was obtained.

$$\frac{t}{Q_t} = \frac{1}{K_2 Q_e^{\,2}} + \frac{1}{Q_e} t \tag{6}$$

Figure 4 shows the simulation results of the IIP dynamics model. It can be seen from the figure that the zero-order kinetic model (R^2 = 0.9966) is more suitable to describe the adsorption kinetic process of the IIP. This means that the IIP is adsorbed layer-by-layer at a constant rate, and the adsorption rate is independent of the concentration of template ions in the adsorption solution, which is similar to the enzymatic reaction process. Because ReO_4^- is excessive in the imprinted hole and the adsorption solution in the IIP, ReO_4^- needs to constantly adjust the direction to enter the imprinted hole to complete the adsorption, which also becomes the speed control step of the entire adsorption process.[50,51]

2.3. Adsorption Thermodynamics of ReO_4^--IIP. The adsorption thermodynamic curve of IIP is shown in Figure 5. It can be seen from the figure that with the increase in the adsorption liquid concentration, the equilibrium adsorption amount (Q_e) gradually increases. When C_e exceeds 0.5 mmol/L, the rate of Q_e increase gradually decreases. After that, the increase in Q_e is gradually decreased until the saturated adsorption capacity was reached. The change in Q_e should be attributed to the transfer between adsorption sites, first. There are different types of adsorption sites in the IIP network, namely, complete imprinted cavities (CICs), imprinting cavities with some defects (ICD), and free active loci (FAL), and the affinities of these sites are different which are in the order CIC > ICD > FAL. Thus, adsorption would start at CICs and terminate at FAL naturally. As the concentration of ReO_4^- was low, the adsorption mainly happened on CICs because of the highest affinity of CICs to ReO_4^-, the equilibrium constant was large relatedly, and Q_e increased with a high degree naturally. As the concentration increases, due to the decrease in the affinity for ReO_4^-, the adsorption gradually shifts to ICD and FAL, the equilibrium constant decreased gradually, and the increase in degree of Q_e decreased gradually.

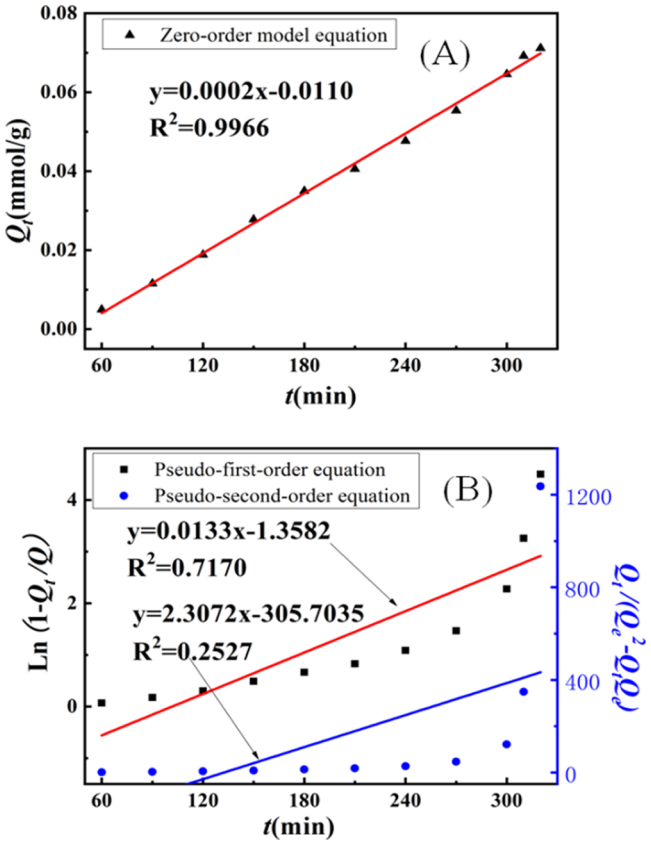

Figure 4. (A) Zero-order kinetic and (B) pseudo-first-order and pseudo-second-order kinetic curve of the IIP for ReO_4^-.

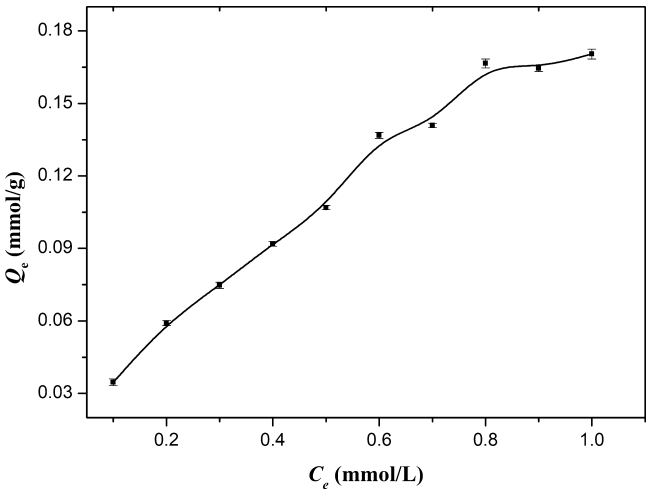

Figure 5. Relationship between adsorption capacity and the concentration of adsorption solution.

In order to verify whether different adsorption sites existed, the adsorption thermodynamic data were simulated using the Scatchard model as shown in eq 7.[51]

https://dx.doi.org/10.1021/acsomega.0c02634
ACS Omega 2020, 5, 24356−24366

$$\frac{Q_e}{C_e} = \frac{Q_m - Q_e}{K_d} \quad (7)$$

thereinto Q_m (mmol/g) delegates the maximum equilibrium adsorption capacity and K_d (mmol/L) is the equilibrium dissociation constant of the binding site.

Figure 6 presents the simulation result of the Scatchard model, and it could have found two different parts of the

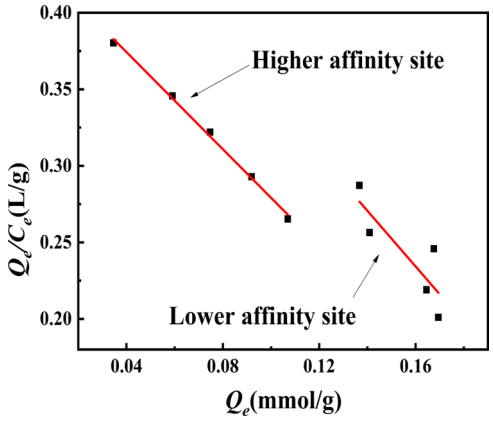

Figure 6. Simulation results of the Scatchard model.

documented Scatchard diagram, suggested that the affinity of binding sites in the IIP to ReO_4^- was different, and ensured that different adsorption sites existed. There are two linear equations for ReO_4^--IIP that could be expressed as follows

$$\frac{Q_e}{C_e} = -1.58601C_e + 0.43774 \qquad R^2 = 0.9956 \quad (8)$$

$$\frac{Q_e}{C_e} = -1.81652C_e + 0.52498 \qquad R^2 = 0.6363 \quad (9)$$

Calculated from the slope and intercept of the equation, the linear equation for high-affinity sites and low-affinity sites is explained in equations. For the higher-affinity site, the values of K_d and Q_m were 0.6305 mmol/L and 0.2735 mmol/g and then the values of K_d and Q_m were 0.5505 mmol/L and 0.2890 mmol/g for low-affinity sites, respectively. By comparing the variance of the two lines, it can be easily concluded that there are more than two binding sites in ReO_4^--IIP, which is due to the low value of R^2 associated with the low-affinity site.

Besides, the Langmuir and Freundlich models were conscripted to explore the adsorption feature of the IIP, and equations are presented as follows[52]

$$\frac{C_e}{Q_e} = \frac{1}{Q_m - k_L} + \frac{C_e}{Q_m} \quad (10)$$

$$\ln Q_e = \frac{\ln C_e}{n} + \ln k_F \quad (11)$$

where k_L and k_F are the adsorption equilibrium constants.

Analyzed results of experimental data using the Langmuir and Freundlich models are shown in Figure 7A,B, respectively. Obviously, the Langmuir model is more suitable to describe the isothermal adsorption characteristics of ReO_4^--IIP, indicating that the adsorption is single-layer adsorption. Because of the high degree of cross-linking, multilayer adsorption hardly occurs.

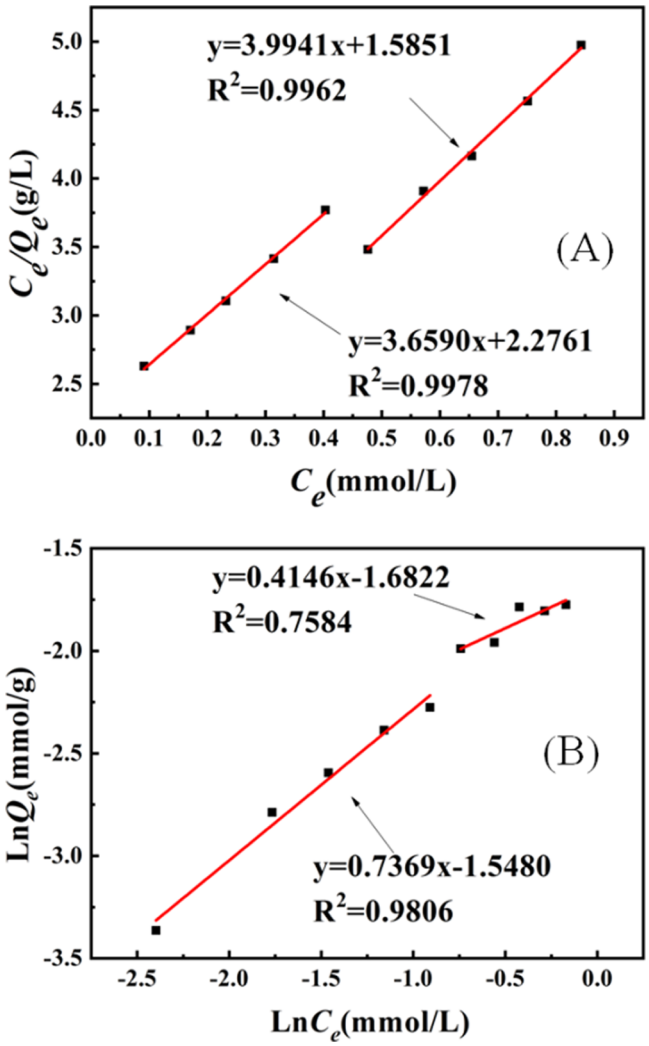

Figure 7. Simulation results of the (A) Langmuir and (B) Freundlich model.

2.4. Influence Factor on Separation and Adsorption Performance of ReO_4^--IIP. For the selectivity study of ReO_4^--IIP, we have considered several heavy metal ions and then MnO_4^- was conscripted as the interference. The main reason is that ReO_4^- and MnO_4^- are similar in spatial structure and shape, and the molecular size of MnO_4^- is smaller than ReO_4^-, so MnO_4^- can enter the imprinted pores of ReO_4^- readily easily. If ReO_4^--IIP can be exhibiting excellent separation performance in the MnO_4^- and ReO_4^- mixture, it can ensure the efficient selection of ReO_4^- in a complex environment. Then, we optimized the process conditions by taking IIP's adsorption capacity and separation degree in the mixed solution of NH_4ReO_4 and $KMnO_4$ at the same molality in the aqueous solution as indicators, and the result is shown in Figure 8.

The effect of n(AA)/n(AM) on separation and adsorption performance of ReO_4^--IIP is explained in Figure 8A. It can be easily seen that as n(AA)/n(AM) increases, Q and R increase first and reach the maximum value when n(AA)/n(AM) = 1.29 and then decrease. The effect of functional monomer self-assembly is determined through the synergy of the functional monomers. When the value of n(AA)/n(AM) is low, the synergy of the functional monomer is not complete, the self-assembly between functional monomers is not complete, and

https://dx.doi.org/10.1021/acsomega.0c02634
ACS Omega 2020, 5, 24356−24366

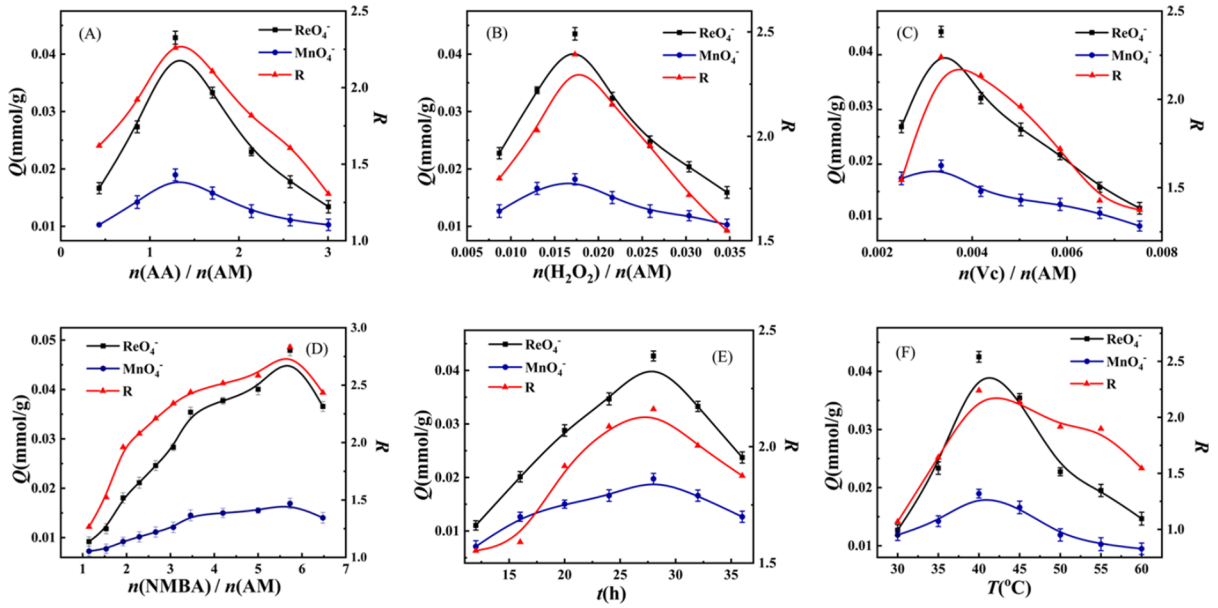

Figure 8. Influence factor on separation performance of ReO_4^--IIP (A) effects of n(AA)/n(AM) under the same other reaction conditions; (B,C) effects of the initiator under the same other reaction conditions; (D) effects of the cross-linking agent under the same other reaction conditions; and (E,F) effects of the reaction time and polymerization temperature under the same other reaction conditions.

the number of free functional groups (FFGs) increases, which leads to the deformation of the imprinted cavity and leads to the increase in the number of dead angle (DA), and the Q and R values are lower. With the increase in n(AA)/n(AM), self-assembly is completed and the number of FFGs decreases, leading to an increase in CICs, reduction in FAL and DA, and fortifying in Q and R. Nevertheless, excessively increasing n(AA)/n(AM) will lead to excess AA, and incomplete self-assembly will occur again. In addition, when the FFG rises, the same as less n(AA)/n(AM), Q and R fall once again. Through Figure 8B, it can be found that with the increase in $n(H_2O_2)$/n(AM), Q and R increase first and then decrease, reaching the maximum when $n(H_2O_2)/n$(AM) = 0.02. When the amount of the initiator involved in the reaction is small, the polymerization speed becomes slacken, and the degree of polymerization and network cross-linking of the product is low, resulting in an incomplete cavity, a large increase in soluble components and FFGs, and a decrease in CICs and effective adsorption sites (EASs). FAL increases. Q and R naturally exhibit low values. When the amount of the initiator is low, the polymerization reaction slows down, the degree of polymerization and network cross-linking becomes low, resulting in incomplete cavity, the soluble components and FFGs in the reactant increase greatly, CICs and EASs decrease, and FAL increases. Q and R exhibit low values quite sensibly. As the relative value of $n(H_2O_2)/n$(AM) increases, the polymerization rate of the reaction, the degree of polymerization, and the degree of cross-linking of the product increase, and the amount of FFGs decreases. Therefore, CICs and EASs in the adsorbent increase, FAL and DA decrease, and Q and R for metal ions naturally increase. When the initiator involved in the reaction increases too much, the reaction rate will fortify promptly, leading to internal explosion of the reaction product and the breakage of the self-assembled structure formed. As shown in the figure, the FFG in the reaction product enhanced additionally. FAL and DA increase, CIC decreases, and Q and R for ReO_4^- decrease unavoidable. Similarly, the trend of change shown in Figure 8C can also be expressed in the abovementioned terms. Vc and H_2O_2 together form the initiation system of the reaction. Obviously, as n(NMBA)/n(AM) increases, Q and R first increase and then decrease, reaching the maximum value at n(NMBA)/n(AM) = 5.73, as shown in Figure 8D. When the amount of the cross-linking agent NMBA is small, the network cross-linking degree of the reaction product is low, resulting in a large amount of the soluble polymer, so the imprinting cavity hardness is low, and the amount of the FFG becomes large. The soluble polymer will be eluted during the drying and adsorption process, and the imprinting cavity will be deformed or collapsed, resulting in a low CIC value of the final reaction product, high FAL and DA values, and low Q and R for ReO_4^-. As the amount of the cross-linking agent NMBA increases, the cross-linking degree and rigidity of ReO_4^--IIP increase so that the content of the soluble polymer FFG decreases, causing FAL and DA to decrease, CIC to increase, and an increase in Q and R for ReO_4^-. Nevertheless, excessive increase in NMBA will excessively increase the degree of cross-linking of the polymer, resulting in an increase in DA and a decrease in CICs. As a result, Q and R will decrease.

The reaction conditions, that is, the influence of polymerization time (t) and polymerization temperature (T) on separation and adsorption performance of ReO_4^--IIP, are shown in Figure 8E,F. It can be seen from Figure 8E that as the polymerization time (t) increases, Q and R first increase and then decrease, reaching a maximum at 28 h. The preparation process of the IIP has two methods: chain polymerization and stepwise polymerization. At the beginning of the polymerization reaction, the chain reaction (polymerization and cross-linking reaction) is incomplete. The reaction product contains a large amount of the soluble polymer, which will lead to an increase in FFGs. As the soluble polymer is extracted and eluted, the imprinted cavity in the adsorbent will subside and deform, EAS will decrease, and the relative amount of FAL and DA will increase. As described, the value of Q is a low value. R naturally records a relatively high value. As the polymerization time increases, the degree of completion of the chain reaction

https://dx.doi.org/10.1021/acsomega.0c02634
ACS Omega 2020, 5, 24356−24366

becomes higher, the degree of ReO_4^--IIP cross-linking increases, FFG decreases, and CIC increases, resulting in a decrease in FAL and DA on the adsorbent. Under this condition, the value of Q increases. For CIC is similar in structure to MnO_4^- and has a small volume, CIC can also absorb MnO_4^- with excellent affinity. When the polymerization time is too long, the dominant reaction of polymerization will gradually turn into a gradual polymerization reaction, which will increase the number of FFG in the IIP. Progressive polymerization is not good for maintaining the shape of the imprinted hole, the imprinted hole will be deformed toward DA; moreover, the value of Q and R will decrease involuntarily. In Figure 8F, it can be clearly seen that as the reaction temperature T increases, the Q and R of the reaction product for ReO_4^- first increase and then decrease, with a peak value of 40 °C. This can be explained by the abovementioned mechanism. As that of the general reaction, polymerization is also needed to overcome active energy, which meant that polymerization could be initiated hardly less than 40 °C; thus, a large quantity of soluble components would have existed in the obtained samples naturally. Because of the removal of soluble components, the self-assembly structure could not be reserved completely, and the content of CIC in the sample was small correspondingly. At the same time, for the removal of template ions in the later stage, soluble components will be removed, thereby increasing the number of FFGs. Because of the strong interaction between FFGs, the matrix will collapse and the imprinted cavity will be deformed or even buried. The results show that the number of EAS in the adsorbent is low, and most of them are FAL and DA. In addition, because of the higher content of DA, the entrance probability of ReO_4^- into DA increased. Because ReO_4^- absorbed by DA could be desorbed hardly. The adsorption capacity and selectivity of the three EAS are different. The low adsorption capacity and selectivity of FAL in the adsorbent make adsorption and desorption more important. The adsorption capacity of DA is high, but the selectivity is poor, and the adsorbed ions are difficult to be desorbed. Although adsorption force and selectivity of CIC were excellent, ions adsorbed in it could be desorbed under suitable conditions. Thus, desorption in the IIP was mainly undertaken by CICs, and the value of R is high relatively. As the temperature increases, the polymerization and cross-linking reactions gradually increase and complete, the amount of soluble FFGs in the reactants gradually decreases, the collapse of the IIP matrix and the deformation of the imprinting cavity gradually decrease spontaneously, the CIC increases, and the FAL and DA decrease. Under this condition, the value of Q and R increase accordingly. When T continues to increase to an inappropriate value, the reaction rate will increase, leading to the self-assembled structure formed by internal explosion and destruction, and FFG increases once again. At lower temperature, the amount of FAL and DA in the adsorbent increases and the CIC decreases. Naturally, the values of Q and R in the adsorbent for ReO_4^- become smaller.

At present, the research on ReO_4^--IIP is barely reported. We can understand almost exclusively the work of our laboratory. The maximum adsorption capacity (Q) of this ReO_4^--IIP was compared with the adsorption results using previous work, as shown in Table 2. The Q and R values for ReO_4^--IIP were higher than our previous work. Although some adsorbents brought the maximum adsorption capacity greater than ReO_4^--IIP,[53,54] however, they had various limitations such as complex or expensive synthetic processes. Besides, most of these studies did not specify the detail with the separation degree. The ReO_4^--IIP not only had a high adsorption capacity and separation degree but was also synthesized using a simple method and under a mild environment, so it had potential for practical industrial production.

Table 2. Maximum Adsorption Capacities and Separation Degree of the ReO_4^--IIP

adsorbent	Q (mmol/g)	R	refs
NVP-ReO_4^--IIP	0.037	2.31	previous work 55
ReO_4^-—IIP	0.064	3.2	this paper

2.5. Reusability of ReO_4^--IIP. Figure 9 shows a columnar schematic diagram of the reusability of the ReO_4^--IIP.

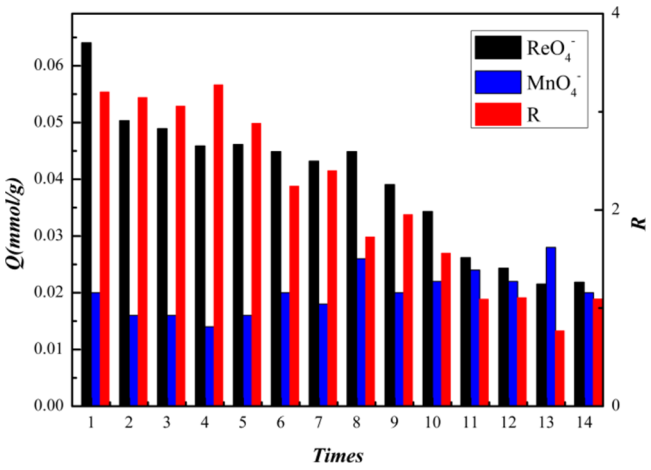

Figure 9. Reusability diagram of the adsorbent.

Obviously, as the number of repetitions increases, $Q_{(ReO_4^-)}$ maintains a certain level at the beginning, and the adsorption capacity drops rapidly after 10 times. Subsequently, the value of $Q_{(ReO_4^-)}$ decreased gradually. As the number of repetitions increases, the value of R gradually decreases. Various indicators show that the ReO_4^--IIP synthesized under the best conditions has an excellent rigid structure to make its reuse optimal. However, it is worth noting that as the number of repetitions increases, the shape of the CIC will deform or collapse gradually, resulting in a decrease in the specific selectivity of the adsorbent. In conclusion, the adsorbent synthesized under optimal conditions has good reusability. Within nine times, there will not be much difference in adsorption and separation capabilities.

3. CONCLUSIONS

The ReO_4^--IIP was prepared by solution polymerization using NH_4ReO_4 as template ions, AA and AM as functional monomers, NMBA as a cross-linker, and H_2O_2-Vc as an initiator. The effects of adsorption selectivity conditions were optimized, and the optimal operation conditions were obtained as follows: the molar ratios of AA, NMBA, H_2O_2, and Vc to AM were 1.29, 5.73, 0.02, and 0.003. The optimal time and temperature of the reaction were 28 h and, 40 °C, respectively. Under the optimum conditions, the ReO_4^--IIP was prepared which exhibited good reusability and selectivity. Besides, through analysis, the Langmuir model and the zero-order kinetic model can describe the adsorption characteristics of the

https://dx.doi.org/10.1021/acsomega.0c02634
ACS Omega 2020, 5, 24356−24366

ReO_4^--IIP better. In addition, the Scatchard model reveals the high binding sites and existence for the ReO_4^--IIP. At last, the morphology and structure of the ReO_4^--IIP were characterized by TEM and Fourier transform infrared spectroscopy (FTIR). The results showed clearly that imprinted cavities had been formed in the ReO_4^--IIP.

4. EXPERIMENTAL SECTION

4.1. Materials. AA (CP, Tianjin Guangfu Co., Ltd.); polyvinyl alcohol (1788, Tianjin Guangfu Co., Ltd.); sodium hydrogen phosphate (Na_2HPO_4, AR, Tianjin Guangfu Co., Ltd.); AM (CP, Henan, Boai Co., Ltd.); ascorbic acid (Vc, AR, Beijing, Deen Co., Ltd.); NMBA (CP, Beijing, Komiiou Reagent Co., Ltd.); hydrogen peroxide (H_2O_2, 30%, Tianjin, Hengxing Co., Ltd.); citric acid (CA, AR, Tianjin, Hengxing Co., Ltd.); methanol (MeOH, AR, Yantai, Guangfu Co., Ltd.); ethanol (EtOH, AR, Shandong, Guangfu Co., Ltd.); potassium permanganate ($KMnO_4$, AR, Changsha, Changrun Co., Ltd.); ammonium perrhenate (NH_4ReO_4, AR, Hunan, Chuangrun Co., Ltd.); ethyl violet (90%, Shanghai, Hongyi Co., Ltd.) were used. Deionized water is prepared using the distiller (YAZDL-10, Qingdao, Juchang Co., Ltd.).

4.2. Maximum Determination of Adsorption Wavelengths. The maximum absorbance wavelength (ReO_4^- or MnO_4^-) was measured using a UV−Vis spectrophotometer (752N, Shanghai Precision and Scientific Instrument Co. Ltd). The maximum absorbance wavelength of ReO_4^- was measured by the ethyl violet method. The maximum absorbance wavelength of MnO_4^- was measured by the direct method. The relationship between the absorbency and wavelength is shown in Figure S1.

4.3. Relationship between Absorbency and Concentration. In the concentration from 0.19 to 0.93 mmol/L, the relationship of absorbance (NH_4ReO_4 and $KMnO_4$) was measured at 658 nm by the violet chromatography method. In the concentration from 0.19 to 0.93 mmol/L, the relationship of absorbance ($KMnO_4$) was measured at 500 nm by the direct method. The results are shown in Figure S2.

To further investigation whether there was interaction between ReO_4^- and MnO_4^-, at the mixed concentration of 0.93 mmol/L, the relationship between absorbency and molar ratio was studied. Figure S3 shows a well linear relationship between absorbency and molar ratio (the range of NH_4ReO_4/$KMnO_4$ was 4/6 to 8/2).

4.4. Synthesis of the ReO_4^--IIP. First, 18.00 mmol AM and 25 mL of methanol and water mixed solution (the volume ratio was 7:3) were added into a 250 mL four-necked flask which was equipped with an outlet tube, constant-pressure funnel, gas inlet, and thermometer. Then, NH_4ReO_4, NMBA, and AM were added into a flask [$n(NH_4ReO_4)/n(AM)$ = 0.052, $n(NMBA)/n(AM)$ = 5.73, and $n(AA)/n(AM)$ = 1.29]. By sealing and fixing the flask on a magnetic stirrer, the solution was magnetic-stirred for 10 min under the purge of nitrogen (N_2). As the time arrived, H_2O_2 and Vc solutions [$n(Vc)/n(AM)$ = 0.003 and $n(H_2O_2)/n(AM)$ = 0.02] were added to the reaction solution. With the reaction progressing, the rotation rate of the magnet went down gradually, until the magnet could not rotate in the flask. Then, the flask was put into a 35 °C water bath for 24 h. When the reaction finished, the polymers were taken out and cut into some fine grained chippings and then these fine grained chippings were baked at 90 °C for 24 h. After the polymers were evaporated, they were broken up and sieved. The 50−150 mesh adsorbent powder was collected and put into a 200 mesh tea bag. The bag was put into a Soxhlet extractor and resinized with 95% alcohol. The polymers were put into an oven under 90 °C until constant weight was achieved and then they were stored in desiccators for further use. The NIIP was prepared following the same procedure but without template ions.

4.5. FTIR Measurements and Characterization of IIP's Morphology. ReO_4^--IIP, NIIP, ReO_4^--IIP after adsorption (used IIP), and ReO_4^--IIP that has been reused nine times (reused IIP) were ground into powder using an agate mortar. FTIR (Nicolet Nexus 670, American Nicolet Co., Ltd., U.S.) was performed. Then, the FTIR test of the samples was performed to determine the components using the KBr pressed-disk method, and the scan wavenumber range was 4000−400 cm^{-1}. The morphology of the IIP was characterized by SEM (JSM-5600LV, JEOL Co., Ltd., Tokyo, Japan) and transmission electron microscope (TEM, TECNAI G^2 TF20, FEI Co., Ltd., U.S.).

4.6. Determination of Adsorption Kinetics. A total of 0.2 g of adsorbents was taken into a tea bag (50 × 7.6 mm, 200 mesh). Then, the tea bag was sealed and placed into a conical flask with 50 mL of NH_4ReO_4 solution (the concentration was 0.75 mmol/L). The conical flask temperature was maintained constant at 30 °C. After certain time, the tea bag was removed and the absorbency of the raffinate was tested using a UV−visible spectrophotometer (ethyl violet method, λ = 658 nm). The value of Q for the adsorbent was calculated according to eq 12

$$Q = \frac{(C_0 - C)}{W} V \tag{12}$$

where Q is the adsorption capacity of the adsorbent (mmol/g), C_0 is the initial concentration of NH_4ReO_4 (mmol/L), C is the NH_4ReO_4 concentration after adsorption at time t (mmol/L), V is the volume of the solution (L), and W is the mass of the adsorbent (g).

4.7. Determination of Adsorption Thermodynamics. A total of 0.1 g of adsorbents was taken into a series of tea bags (50 × 7.6 mm, 200 mesh). Then, the tea bags were sealed and placed into conical flasks with 30 mL of NH_4ReO_4 solution (the concentration were 0.1−1 mmol/L, severally). The conical flask temperature was maintained constant at 30 °C. After 5.5 h, the tea bag was removed and the absorbency of the raffinate was tested using a UV−visible spectrophotometer (ethyl violet method, λ = 658 nm). Q_e was calculated using eq 13.

$$Q_e = \frac{(C_0 - C_e)}{W} V \tag{13}$$

where Q_e is the equilibrium adsorption capacity of the adsorbent (mmol/g) and C_e is the equilibrium concentration of NH_4ReO_4 (mmol/L).

4.8. Determination of Adsorption Capacity. A total of 0.2 g of adsorbents was taken into a tea bag (50 × 7.6 mm, 200 mesh). Then, the tea bag was sealed and placed into a conical flask with 50 mL of NH_4ReO_4 and $KMnO_4$ solution (the concentration both as 0.75 mmol/L). The conical flask temperature was maintained constant at 30 °C. After adsorption to equilibrium, the tea bag was removed and the absorbency of the raffinate was tested using a UV−visible spectrophotometer (λ = 658 nm, ethyl violet method and λ = 500 nm, direct method). The value of Q for the adsorbent

https://dx.doi.org/10.1021/acsomega.0c02634
ACS Omega 2020, 5, 24356−24366

toward ReO_4^- or MnO_4^- was calculated according to eqs 14 and 15

$$Q_{(ReO_4^-)} = \frac{(C_{0(ReO_4^-)} - C_{(ReO_4^-)})}{W} V \quad (14)$$

$$Q_{(MnO_4^-)} = \frac{(C_{0(MnO_4^-)} - C_{(MnO_4^-)})}{W} V \quad (15)$$

where $Q_{(ReO_4^-)}$ and $Q_{(MnO_4^-)}$ are the adsorption capacities of ReO_4^- and MnO_4^- when the adsorption achieved equilibrium (mmol/g), respectively; $C_0(ReO_4^-)$ and $C_0(MnO_4^-)$ are the initial concentration of ReO_4^- and MnO_4^- (mmol/L); and $C_{(ReO_4^-)}$ and $C_{(MnO_4^-)}$ are the raffinate concentration of ReO_4^- and MnO_4^- (mmol/L), respectively.

4.9. Calculation of the Separation Degree. After a cycle of adsorption, the $Q_{(ReO_4^-)}$ and $Q_{(MnO_4^-)}$ were measured and the separation degree (R) was calculated according to eq 16

$$R = \frac{Q_{(ReO_4^-)}}{Q_{(MnO_4^-)}} \quad (16)$$

4.10. Reusability of the ReO_4^--IIP. The adsorption and desorption were repeated several times. $Q_{(ReO_4^-)}$, $Q_{(MnO_4^-)}$, and R values were measured and calculated.

■ ASSOCIATED CONTENT

Supporting Information

The Supporting Information is available free of charge at https://pubs.acs.org/doi/10.1021/acsomega.0c02634.

Relationship between the absorbency and wavelength of ReO_4^- and MnO_4^- with the ethyl violet photometry method and direct measure; standard curve of ReO_4^- and MnO_4^- at 658 nm with the ethyl violet photometry method and MnO_4^- at 500 nm under the direct measurement method; and relationship between the absorbency and molar ratio (A) of $NH_4ReO_4/KMnO_4$ (PDF)

■ AUTHOR INFORMATION

Corresponding Author

Zhenbin Chen − *State Key Laboratory of Advanced Processing and Recycling of Nonferrous Metals and School of Materials Science and Engineering, Lanzhou University of Technology, Lanzhou 730050, Gansu, China*; Email: zhenbinchen@163.com

Authors

Pu Liu − *State Key Laboratory of Advanced Processing and Recycling of Nonferrous Metals and School of Materials Science and Engineering, Lanzhou University of Technology, Lanzhou 730050, Gansu, China; Baiyin Research Institute of Novel Materials of Lanzhou University of Technology, Baiyin 730900, Gansu, China*

Weiwei Jia − *State Key Laboratory of Advanced Processing and Recycling of Nonferrous Metals and School of Materials Science and Engineering, Lanzhou University of Technology, Lanzhou 730050, Gansu, China*

Xiaojian Ou − *State Key Laboratory of Nickel and Cobalt Resources Comprehensive Utilization, Jinchang 737100, Gansu, China*

Chunli Liu − *State Key Laboratory of Advanced Processing and Recycling of Nonferrous Metals and School of Materials Science and Engineering, Lanzhou University of Technology, Lanzhou 730050, Gansu, China*

Jun Zhang − *State Key Laboratory of Advanced Processing and Recycling of Nonferrous Metals and School of Materials Science and Engineering, Lanzhou University of Technology, Lanzhou 730050, Gansu, China*; orcid.org/0000-0003-2121-4510

Xiaoming Li − *Baiyin Research Institute of Novel Materials of Lanzhou University of Technology, Baiyin 730900, Gansu, China*

Complete contact information is available at: https://pubs.acs.org/10.1021/acsomega.0c02634

Author Contributions

⊥P.L. and W.J. contributed to this work equally.

Notes

The authors declare no competing financial interest.

■ ACKNOWLEDGMENTS

This work was supported by the National Natural Science Foundation, China (grant: 51061009), Shenyang National Laboratory for Materials Science and State Key Laboratory of Advanced Processing and Recycling of Nonferrous Metals (18LHPY004 and 18LHZD003), and Open Project of State Key Laboratory of Nickel and Cobalt Resources Comprehensive Utilization (2019-16).

■ REFERENCES

(1) Guo, J.; He, X.; Huan, W. Reviews of Metallurgical Technology to Recovery Platinum Group Metals from Secondary Resource in China. *Precious Met.* **2012**, *33*, 18−23.

(2) Xin, Z.; Run, B.; Donghui, W.; Xiaomei, C.; Feng, W. Research Development of Refractory Metal Materials Used in the Field of Aerospace. *Rare Met. Mater. Eng.* **2011**, *40*, 1871−1875.

(3) Luo, Y. S.; Liu, S. Z.; Sun, F. L. Research Status of Strengthening Mechanism of Germanium in Single Crystal Superalloy. *Mat Guide* **2005**, *19*, 55−58.

(4) Kobayashi, T.; Koizumi, Y.; Yokokawa, T.; Osawa, M.; Harada, H.; Maruko, T. Development of 4th generation sc superalloys without Re. *Nippon Kinzoku Gakkaishi* **2005**, *69*, 272−275.

(5) Ernst, F.; Michael, M.; Ernst, A. Quantitative experimental determination of the solid solution hardening potential of rhenium, tungsten and molybdenum in single-crystal nickel-based superalloys. *Acta Mater.* **2015**, *87*, 350−356.

(6) Lakowicz, J. R.; Nair, R.; Piszczek, G.; Gryczynski, I. End to end diffusion on the microsecond timescale measured with resonance energy transfer from a long-lifetime rhenium metal-ligand complex. *Photochem. Photobiol.* **2000**, *71*, 157.

(7) Fang, D.-w.; Song, Z.-r.; Zhang, S.-c.; Li, J.; Zang, S.-l. Solvent Extraction of Rhenium(VII) from Aqueous Solution Assisted by Hydrophobic Ionic Liquid. *J. Chem. Eng. Data* **2017**, *62*, 1094−1098.

(8) Gu, Y.; Zhang, Y.; Lin, L.; Xu, H.; Orndorff, W.; Pan, W.-P. Evaluation of elemental mercury adsorption by fly ash modified with ammonium bromide. *J. Therm. Anal. Calorim.* **2015**, *119*, 1663−1672.

(9) Hu, Q.; Liu, L.; Zhao, X.-b.; Gao, S.-f.; Zhang, J.; Fu, H.-z. Effect of carbon and boron additions on segregation behavior of directionally solidified nickel-base superalloys with rhenium. *Trans. Nonferrous Met. Soc. China* **2013**, *23*, 3257−3264.

(10) Balamurugan, K.; Gokulakrishnan, K.; Prakasam, T. Preparation and evaluation of molecularly imprinted polymer liquid chromatography column for the separation of Cathine enantiomers. *Saudi Pharm. J.* **2012**, *20*, 53−61.

(11) Yang, T.; Liu, L. H.; Liu, J. W. Cyanobacterium metallothionein decorated graphene oxide nanosheets for highly selective adsorption of ultra-trace cadmium. *J. Mater. Chem.* **2012**, *22*, 21909.
(12) Sirimaneetham, V.; Temple, J. R. W. Macroeconomic Stability and the Distribution of Growth Rates. *World Bank Econ. Rev.* **2009**, *23*, 443−479.
(13) Xi, Y.; Luo, Y.; Luo, J.; Luo, X. Removal of Cadmium(II) from Waste water Using Novel Cadmium Ion-Imprinted Polymers. *J. Chem. Eng. Data* **2015**, *60*, 3253−3261.
(14) Zhang, J.; Wang, M.; Peng, W.; Chen, Z.; Chen, Z. Glutathione Surface Molecularly Imprinted Polymer from CLX1180 via Three Modes of Polymerization for Selective Adsorption of Glutathione. *ACS Omega* **2020**, *5*, 13777−13784.
(15) Zhang, W.; Yun, M.; Yu, Z.; Chen, D.; Li, X. A Novel Cu (II) Ion-Imprinted Alginate−Chitosan Complex Adsorbent for Selective Separation of Cu (II) from Aqueous Solution. *Polym. Bull.* **2019**, *76*, 1861−1876.
(16) Layet, C.; Santaella, C.; Auffan, M.; Chevassus-Rosset, C.; Montes, M.; Levard, C.; Ortet, P.; Barakat, M.; Doelsch, E. Phytoavailability of silver at predicted environmental concentrations: does the initial ionic or nanoparticulate form matter. *Environ. Sci.: Nano* **2019**, *6*, 127−135.
(17) Shao, P.; Ding, L.; Luo, J.; Luo, Y.; You, D.; Zhang, Q.; Luo, X. Lattice defect enhanced adsorption of arsenic on zirconia nanospheres: a combined experimental and theoretical study. *ACS Appl. Mater. Interfaces* **2019**, *11*, 29736−29745.
(18) Chen, X.; Tan, Z..; Feng, Yu.; Li, B..; Guo, Z..; Ru, B.. Recent progress of recovery of scattered metal rhenium from high-temperature alloy scrap. *Mod. Chlor-Alkali Technol.* **2017**, *37*, 60−63.
(19) Lin, M.; Feng, C.; Li, M.; Zeng, Q.; Gan, Q. Synthesis and application of a surface-grafted In (III) ion-imprinted polymer for selective separation and pre-concentration of indium (III) ion from aqueous solution. *Hydrometallurgy* **2015**, *154*, 63−71.
(20) Shamsipur, M.; Rajabi, H. R. Flame photometric determination of cesium ion after its preconcentration with nanoparticles imprinted with the cesium-dibenzo-24-crown-8 complex. *Mikrochim. Acta* **2013**, *180*, 243−252.
(21) Rajabi, H. R.; Razmpour, S. Synthesis, characterization and application of ion imprinted polymeric nanobeads for highly selective preconcentration and spectrophotometric determination of Ni(2+) ion in water samples. *Spectrochim. Acta, Part A* **2016**, *153*, 45−52.
(22) Haaf, F.; Sanner, A.; Straub, F. Polymers of N-Vinyl-pyrrolidone: Synthesis, Characterization and Uses. *Polym. J.* **1985**, *17*, 143−152.
(23) Asgharinezhad, A. A.; Jalilian, N.; Ebrahimzadeh, H.; Panjali, Z. A simple and fast method based on new magnetic ion imprinted polymer nanoparticles for the selective extraction of Ni(II) ions in different food samples. *RSC Adv.* **2015**, *5*, 45510−45519.
(24) Gao, B.; Du, J.; Zhang, Y. Preparation of Arsenate Anion Surface-Imprinted Material IIP-PDMC/SiO_2 and Study on Its Ion Recognition Property. *Ind. Eng. Chem. Res.* **2013**, *52*, 7651−7659.
(25) Zhou, Z.; Kong, D.; Zhu, H.; Wang, N.; Wang, Z.; Wang, Q.; Liu, W.; Li, Q.; Zhang, W.; Ren, Z. Preparation and adsorption characteristics of an ion-imprinted polymer for fast removal of Ni(II) ions from aqueous solution. *J. Hazard. Mater.* **2018**, *341*, 355.
(26) Yu, H.; Shao, P.; Fang, L.; Pei, J.; Ding, L.; Pavlostathis, S. G.; Luo, X. Palladium ion-imprinted polymers with PHEMA polymer brushes: Role of grafting polymerization degree in anti-interference. *Chem. Eng. J.* **2019**, *359*, 176−185.
(27) Yin, X.; Shao, P.; Ding, L.; Xi, Y.; Zhang, K.; Yang, L.; Shi, H.; Luo, X. Protonation of rhodanine polymers for enhancing the capture and recovery of Ag^+ from highly acidic wastewater. *Environ. Sci.: Nano* **2019**, *6*, 3307−3315.
(28) Yin, X.; Long, J.; Xi, Y.; Luo, X. Recovery of silver from wastewater using a new magnetic photocatalytic ion imprinted polymer. *ACS Sustainable Chem. Eng.* **2017**, *5*, 2090−2097.
(29) Felix, C. S. A.; Silva, D. G.; Andrade, H. M. C.; Riatto, V. B.; Victor, M. M.; Ferreira, S. L. C. An on-line system using ion-imprinted polymer for preconcentration and determination of bismuth in seawater employing atomic fluorescence spectrometry. *Talanta* **2018**, *184*, 87−92.
(30) Min, X.; Wu, X.; Shao, P.; et al. Ultra-high capacity of lanthanum-doped UiO-66 for phosphate capture: Unusual doping of lanthanum by the reduction of coordination number. *Chem. Eng. J.* **2019**, *358*, 321−330.
(31) Zhai, Y.; Liu, Y.; Chang, X. Metal ion-small molecule complex imprinted polymer membranes: Preparation and separation characteristics. *React. Funct. Polym.* **2008**, *68*, 284−291.
(32) Fereidoonipour, F.; Rajabi, H. R. Development of flow injection analysis-solid phase extraction based on ion imprinted polymeric nanoparticles as an efficient and selective technique for preconcentration of zinc ions from aqueous solution. *New J. Chem.* **2017**, *41*, 8828−8836.
(33) Roushani, M.; Saedi, Z.; Hamdi, F. Application of ion-imprinted polymer synthesized by precipitation polymerization as an efficient and selective sorbent for separation and pre-concentration of chromium ions from some real samples. *J. Iran. Chem. Soc.* **2018**, *15*, 2241−2249.
(34) Acharya, A.; Mohan, H.; Sabharwal, S. Radiation chemical studies on thermosensitive N-isopropylacrylamide and its polymer in aqueous solutions. *J. Radiat. Res.* **2003**, *44*, 335−343.
(35) Song, X. F.; He, T. S. Resistance to Carbonation of Concrete Treated by Superabsorbent Resin Synthesized In Situ. *Jianzhu Cailiao Xuebao* **2011**, *374−377*, 1872−1876.
(36) Ikemura, K.; Kojima, K.; Endo, T.; Kadoma, Y. Effect of the combination of dithiooctanoate monomers and acidic adhesive monomers on adhesion to precious metals, precious metal alloys and non-precious metal alloys. *Dent. Mater. J.* **2011**, *30*, 469.
(37) Lin, T.; Guan, Q.; Zhang, S. Studies on the separation and purification of total flavones from Lamiophlomis rotata by macroreticular resin. *Chin. Pharm. J.* **2005**, *40*, 264−267.
(38) Zhao, Y.; Chen, Z.; Liu, D.; Long, J.; Di, D. Separation of flavonoids in the leaves of Sophora japonica by macroporous adsorption resin mixed-bed technology. *Pigm. Resin Technol.* **2017**, *46*, 235−243.
(39) Maeda, Y.; Yamamoto, H.; Ikeda, I. Effects of ionization on the phase behavior of poly(N -isopropylacrylamide-co-acrylic acid) and poly(N, N -diethylacrylamide-co-acrylic acid) in water. *Colloid Polym. Sci.* **2004**, *282*, 1268−1273.
(40) Ros, T. G.; van, D. A. J.; Geus, J. W. Surface oxidation of carbon nanofibres. *Chem.—Eur. J.* **2002**, *8*, 1151−1162.
(41) Chen, L.; Liu, J.; Zeng, Q.; Wang, H.; Yu, A.; Zhang, H.; Ding, L. Preparation of magnetic molecularly imprinted polymer for the separation of tetracycline antibiotics from egg and tissue samples. *J. Chromatogr. A* **2009**, *1216*, 3710−3719.
(42) Arras, L. D.; Guthrie, B. S.; Alper, S. Using RNA-interference to Investigate the Innate Immune Response in Mouse Macrophages. *J. Visualized Exp.* **2014**, *93*, e51306.
(43) Guo, B.; Deng, F.; Zhao, Y.; Luo, X.; Luo, S.; Au, C. Magnetic ion-imprinted and−SH functionalized polymer for selective removal of Pb (II) from aqueous samples. *Appl. Surf. Sci.* **2014**, *292*, 438−446.
(44) Deng, G.-C.; Teng, H.-H.; Zhang, Y.-Y.; Zhao, L.-Y.; Wei, M.; Wang, Y.-J.; Zang, S.-L. Spectrophotometric determination of trace rhenium in molybdenum samples using the system of ReO_4^--ethyl violet-polyvinyl alcohol. *Metal Anal.* **2006**, *26*, 27−29.
(45) Fang, P.; Xia, W.; Zhou, Y.; Ai, Z.; Yin, W.; Xia, M.; Yue, Q. Ion-imprinted mesoporous silica/magnetic graphene oxide composites functionalized with Schiff-base for selective Cu(II) capture and simultaneously being transformed as a robust heterogeneous catalyst. *Chem. Eng. J.* **2020**, *385*, 123847.
(46) Samah, N. A.; Rosli, N. A. M.; Manap, A. H. A.; Aziz, Y. F. A.; Yusoff, M. M. Synthesis & characterization of ion imprinted polymer for arsenic removal from water: a value addition to the groundwater resources. *Chem. Eng. J.* **2020**, *394*, 124900.
(47) Tanodekaew, S.; Prasitsilp, M.; Swasdison, S.; Thavornyutikarn, B.; Pothsree, T.; Pateepasen, R. Preparation of acrylic grafted chitin for wound dressing application. *Biomaterials* **2004**, *25*, 1453−1460.

https://dx.doi.org/10.1021/acsomega.0c02634
ACS Omega 2020, 5, 24356−24366

(48) Alizadeh, T.; Atayi, K. Synthesis of hydrogen phosphate anion-imprinted polymer via emulsion polymerization and its use as the recognition element of graphene/graphite paste potentiometric electrode. *Mater. Chem. Phys.* **2018**, *209*, 180−187.
(49) Nakhjiri, M. T.; Marandi, G. B.; Kurdtabar, M. Poly(AA-co-VPA) hydrogel cross-linked with N -maleyl chitosan as dye adsorbent: isotherms, kinetics and thermodynamic investigation. *Int. J. Biol. Macromol.* **2018**, *117*, 152−166.
(50) Valderrama, C.; Cortina, J. L.; Farran, A.; Gamisans, X.; de las Heras, F. X. Kinetic study of acid red "dye" removal by activated carbon and hyper-cross-linked polymeric sorbents macronet Hypersol MN200 and MN300. *React. Funct. Polym.* **2008**, *68*, 718−731.
(51) Matsui, J.; Miyoshi, Y.; Doblhoff-Dier, O.; Takeuchi, T. A molecularly imprinted synthetic polymer receptor selective for atrazine. *Anal. Chem.* **1995**, *67*, 4404−4408.
(52) Niu, Y.; Qu, R.; Chen, H.; Mu, L.; Liu, X.; Wang, T.; Zhang, Y.; Sun, C. Synthesis of silica gel supported salicylaldehyde modified PAMAM dendrimers for the effective removal of hg (II) from aqueous solution. *J. Hazard. Mater.* **2014**, *278*, 267−278.
(53) Li, J.; Chen, C.; Zhang, R.; Wang, X. Reductive immobilization of Re(VII) by graphene modifified nanoscale zero-valent iron particles using a plasma technique. *Sci. China Chem.* **2016**, *59*, 150−158.
(54) Li, Y.; Yang, L.; Liu, X.; Li, N.; Zhang, L.; Li, Q.; Yang, Y.; Duan, Y.; Zhang, F. Highly enhanced selectivity for the separation of rhenium and molybdenum using amino-functionalized magnetic Cu-ferrites. *J. Mater. Sci.* **2015**, *50*, 5960−5969.
(55) Zhang, X.; Jia, W.; Li, D.; Liu, C.; Wang, R.; Li, K.; Li, H.; Chen, Z.; Sun, Y.; Liu, Z. Study on Synthesis and Adsorption Properties of ReO_4^- Ion Imprinted Polymer. *J. Polym. Res.* **2020**, *27*, 201.

https://dx.doi.org/10.1021/acsomega.0c02634
ACS Omega 2020, 5, 24356−24366